Factor B structure provides insights into activation of the central protease of the complement system

Fin J Milder[1], Lucio Gomes[1], Arie Schouten[1], Bert J C Janssen[1], Eric G Huizinga[1], Roland A Romijn[2], Wieger Hemrika[2], Anja Roos[3], Mohamed R Daha[3] & Piet Gros[1]

Factor B is the central protease of the complement system of immune defense. Here, we present the crystal structure of human factor B at 2.3-Å resolution, which reveals how the five-domain proenzyme is kept securely inactive. The canonical activation helix of the Von Willebrand factor A (VWA) domain is displaced by a helix from the preceding domain linker. The two helices conformationally link the scissile-activation peptide and the metal ion–dependent adhesion site required for binding of the ligand C3b. The data suggest that C3b binding displaces the three N-terminal control domains and reshuffles the two central helices. Reshuffling of the helices releases the scissile bond for final proteolytic activation and generates a new interface between the VWA domain and the serine protease domain. This allosteric mechanism is crucial for tight regulation of the complement-amplification step in the immune response.

Factor B is a tightly regulated, highly specific serine protease. In its activated form, it catalyzes the central amplification step of complement activation to initiate inflammatory responses, cell lysis, phagocytosis and B-cell stimulation[1,2]. Factor B is activated through an assembly process: it binds surface-bound C3b, or its fluid-phase counterpart C3(H_2O), after which it is cleaved by factor D into fragments Ba (residues 1–234) and Bb (residues 235–739)[3,4]. Fragment Ba dissociates from the complex, leaving behind the alternative pathway C3 convertase complex C3b–Bb, which cleaves C3 into C3a and C3b (see **Fig. 1a**). This protease complex is intrinsically unstable. Once dissociated from the complex, Bb cannot reassociate with C3b[5]. A similar C3 convertase complex is formed upon activation of the classical (antibody-mediated) and lectin-binding pathways, comprised of C4 and C2, which are homologous to C3 and factor B, respectively. The proenzyme factor B consists of three N-terminal complement control protein (CCP) domains, connected by a 45-residue linker to a VWA domain and a C-terminal serine protease (SP) domain, which carries the catalytic center (**Fig. 1a**). The VWA and SP domains form fragment Bb, and CCP1 through CCP3 and the linker form fragment Ba. Binding of factor B to C3b depends on elements in fragment Ba[6] and the Mg^{2+}-dependent metal ion–dependent adhesion site (MIDAS) motif in the VWA domain of fragment Bb[7]. The VWA domain is structurally homologous to inserted (I) domains in integrins. In I domains, ligand binding to the MIDAS is coupled to a ∼10-Å shift of the α7 activation helix, with concomitant domain rearrangements that activate the integrins[8,9]. Structures of a truncated Bb fragment[10] and its full-length homolog C2a[11] show variable positions of the α7 activation helix affecting

the orientation of the VWA and SP domains, which indicates that a related mechanism may occur in convertase formation and dissociation. These structures, however, do not reveal the regulation of the proteolytic activity of factor B. In particular, it is unclear how factor B is maintained in its inactive, zymogen state and how C3b binding makes factor B susceptible to proteolytic activation by factor D. To gain insights into the regulatory mechanisms underlying complement activation, we set out to determine the structure of human proenzyme factor B.

RESULTS

Overall structure of factor B

Here we present the crystal structure of human proenzyme factor B at 2.3-Å resolution (see Methods and **Supplementary Fig. 1** online). The overall structure (**Fig. 1b**) consists of three lobes, which is in agreement with electron micrographs[12]. One lobe represents the trypsin-like SP domain with the catalytic site in a fully exposed position. The other two lobes represent the VWA domain, with its α/β/α fold, and the CCP1–CCP3 domains, with their typical β-sandwich fold stabilized by pairs of disulphide bonds. The long CCP3-VWA linker, containing the Arg234-Lys235 scissile bond, forms a short loop (residues 198–201), an α-helix (residues 202–213) and a long loop (residues 214–242), which is partially disordered (residues 219–232 are not evident in the electron density). Unexpectedly, the observed linker helix, denoted αL, is integrated into the VWA domain and occupies the position of the α7 activation helix in fragment Bb[10] (**Fig. 2a**). The displaced α7 helix lies adjacent to αL on the surface of the VWA domain. These two helices lie at the center of the five-domain

[1]Crystal and Structural Chemistry, Bijvoet Center for Biomolecular Research, Faculty of Sciences, and [2]ABC Expression Center, Utrecht University, Padualaan 8, 3584 CH Utrecht, The Netherlands. [3]Department of Nephrology, Leiden University Medical Center, 2300 RC Leiden, The Netherlands. Correspondence should be addressed to P.G. (p.gros@chem.uu.nl).
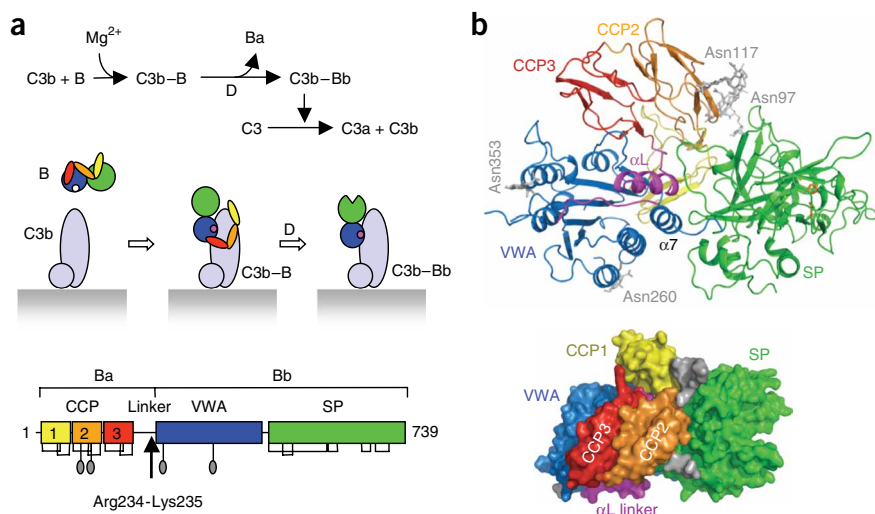
Figure 1 C3 convertase formation and crystal structure of complement factor B. (**a**) Top and middle diagrams, schematic and cartoon representation (based on crystal structure[33,34]) of C3 convertase formation. Bottom diagram, domain topology of factor B; indicated are the N-linked glycans, the disulphide bridges and the Arg234-Lys235 scissile bond. (**b**) Top, structure of factor B shown as ribbons, colored by domain as in **a**. The linker connecting CCP3 and VWA is colored purple. The N-linked glycans (gray) and the catalytic triad Asp-His-Ser (brown) are shown as sticks. Labels indicate the centrally positioned helices αL and α7. Bottom, factor B shown in surface representation (rotated 90° with respect to the top structure).

molecule and affect the domain-domain arrangement (**Fig. 1b**). They provide a conformational link between two key regulatory sites of the molecule: the Mg^{2+}-dependent C3b-binding MIDAS on one side and the activation scissile bond Arg234-Lys235 on the opposite side of the molecule.

VWA domain adopts locked conformation

The VWA domain in factor B adopts an inactive conformation with a displaced helix α7 and distorted MIDAS, which we refer to as a 'locked' conformation. The inactive-closed and active-open conformational states of the VWA and I domains are characterized pre-

dominantly by the conformations of loop βF-α7, helix α7 and the neighboring helix α1 (**Fig. 2b**)[8,13]. In factor B, helix α7 is displaced from its normal binding groove by helix αL (**Fig. 2a**). The preceding loop, βF-α7, adopts a canonical closed conformation, as shown by the positions of its hydrophobic ratchet residues (Val430 and Leu436; see **Fig. 2b** and **Supplementary Fig. 2** online). Helix α1 is also positioned in the inactive-closed conformation. Thus, the unliganded VWA domain has an inactive conformation, as would be expected for the proenzyme state of factor B. Moreover, helix αL obstructs the α7 activation helix, preventing it from taking its normal position in VWA and I domains[8,10,11,13–15], thereby locking the VWA domain in its inactive conformation. Typically, a closed-inactive domain conformation is coupled to a MIDAS conformation with a low affinity for ligands. In factor B,

Figure 2 Regulatory elements in the VWA domain. (**a**) Dislocation of helix α7 by helix αL. Left, overlay of the VWA domains of factor B and fragment Bb (PDB 1RRK) shows the displacement of helix α7 (blue in factor B, green in Bb) by linker helix αL (purple). Right, stereo figure shows the packing of helices α7 and αL against the body of the VWA domain of factor B (gray, surface representation). Hydrophobic residues of helices αL (B) and α7 (Bb) are shown in ball-and-stick representation. (**b**) Conformations of loop βF-α7 and helices α7 and α1. Left image, overlay of VWA domains of factor B (blue) with closed (green; PDB 1AOX) and open (yellow; PDB 1DZI) conformations of the α2 I domain, showing strand βF and helix α7. Middle two images, positions of hydrophobic 'ratchet' residues (sticks) of loop βF-α7 and helix α7. Right image, position of helix α1. (**c**) Distortion of the Mg^{2+}-dependent MIDAS C3b binding site. Left, superposition of the MIDAS motif in factor B (blue) and in Bb (gray), shown in ball-and-stick representation. Gray spheres represent water molecules (small spheres) and the bound ion (large sphere) as observed in Bb. Right, orientation of CCP1 (yellow) and VWA (blue) in factor B, with the VWA domain of Bb (gray) superposed. Shown in ball-and-stick representation are the adjoining residues Gln28 and Asp254 and the glycosylation site Asn260. (**d**) The P1 residue of the buried scissile bond (Arg234-Lys235) interacts with helices α7 (blue) and linker helix αL (purple) via salt bridges.
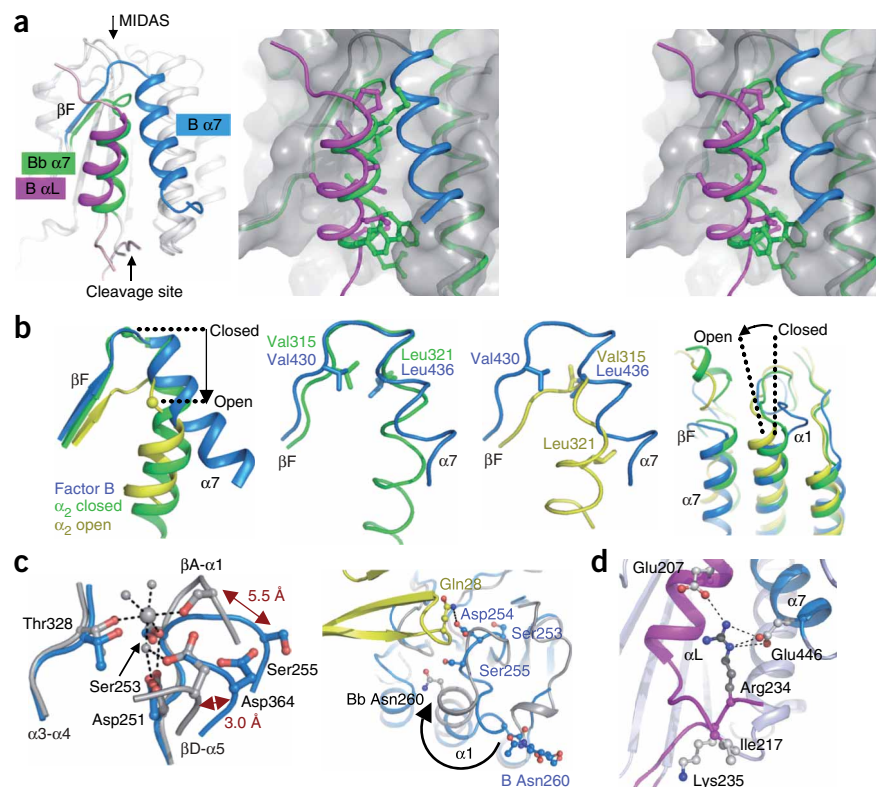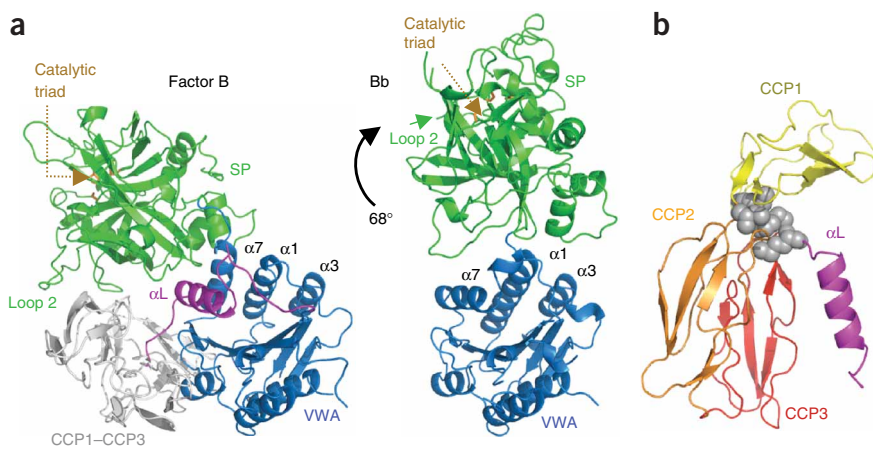
Figure 3 Domain orientations in factor B and Bb. (**a**) Left, orientation of VWA (blue) and SP (green) in factor B with linker and linker helix αL shown in purple and CCP1–CCP3 domains in gray. Right, orientation of VWA and SP in Bb (PDB 1RRK). Indicated are helices αL, α1, α3 and α7, which are involved in the VWA-SP interfaces. (**b**) The CCP triad arrangement in ribbon representation, with CCP1 in yellow, CCP2 in orange and CCP3 in red. Gray spheres indicate the four residues (Tyr42, Ile76, Phe197 and Met198) forming the hydrophobic triad center. The adjoining linker containing helix αL is colored purple.

compared with fragment Bb, displacements up to 5.5 Å in loops βA-α1 and βD-α5 distort the MIDAS (**Fig. 2c** and **Supplementary Fig. 2**). The distorted conformation indicates reduced divalent-ion binding. Moreover, we did not observe electron density for an ion bound to the MIDAS in factor B. The absence of an ion is consistent with the notion that fragment Bb, but not factor B, has high affinity for divalent ions[16]. The neighboring CCP1 domain may affect the MIDAS conformation. Gln28 of loop β2-β3 in CCP1 makes a hydrogen bond to Asp254, located in the displaced VWA βA-α1 loop. Furthermore, CCP1 may prevent loop βA-α1 from assuming the conformation seen in Bb by obstructing the glycan at Asn260. Instead, in factor B helix α1 is shifted and partially unwound, pointing the glycan on Asn260 away from the neighboring CCP1 domain (**Fig. 2c**). Factor B with D254G and N260D single and double mutations (where N260D deletes the N-glycosylation site) forms convertases more readily and more stably than wild-type factor B[17,18], indicating that these mutations promote the transition from an inactive to an active conformation of the VWA domain.

Central role for linker region
The CCP3-VWA linker helix αL occupies the position of helix α7 of the VWA domain. It binds Arg234 of the scissile bond, preventing proteolytic activation. By virtue of its short-chain hydrophobic residues, helix αL is squeezed between helix α7 and the VWA core, effectively blocking helix α7 (**Fig. 2a**). After helix αL, the CCP3-VWA linker forms a long loop and folds back to the C-terminal end of helix αL (**Fig. 2d**). The scissile bond Arg234-Lys235 is located here, buried by the preceding flexible loop. The side chain of Arg234, crucial for substrate binding at the S1 pocket (as defined in Schechter and Berger notation) of factor D, is bound to both helix αL (Glu207) and helix α7 (Glu446) by salt bridges (**Fig. 2d**). Thus, the scissile bond in factor B is protected from proteolysis by factor D and is conformationally linked to helices αL and α7. In contrast, the scissile bond in isolated VWA domains is susceptible to factor D cleavage[19], because they lack the αL-α7 arrangement that locks the P1 residue (Arg234). In the formation of the convertase, binding of C3b to factor

B probably induces reshuffling of helices αL and α7 that liberates the P1 arginine residue and makes the scissile bond accessible for proteolysis by factor D.

Conformation of the catalytic SP domain
In both factor B and fragment Bb[10], the SP domain is exposed and the catalytic site is freely accessible to small substrates[20]. The two structures differ markedly in the orientation of the VWA-SP region (**Fig. 3a**). In factor B, the VWA-SP interface is dominated by helices αL and α7, with the N-terminal loop of SP folding over helix αL; furthermore, contacts are observed between SP and domains CCP1 and CCP2. In fragment Bb, where αL and the CCP1–CCP3 domains are absent, SP rotates 68° and contacts helices α7, α1 and α3 of the VWA domain. In addition to the interface loops, loop 2 of the SP domain is markedly different in factor B and fragment Bb. Putatively, Arg705 of this loop (like Arg696 in C2a[11]) induces formation of the oxyanion hole, similar to the N terminus in trypsin after proteolytic activation of trypsinogen[21]. Consistent with this model, the guanidinium group of the arginine interacts with an aspartate of the oxyanion-hole loop in Bb and C2a (**Supplementary Fig. 3** online). In factor B, loop 2 folds back toward the N-glycosylated Asn97 on CCP2 (weak electron density for the side chains indicates disorder in loop 2). Concomitantly, the guanidinium group of Arg705 is displaced by 11 Å, as would be expected for the zymogen state. Nevertheless, the conformation of the oxyanion hole is identical between factor B and fragment Bb—that is, in factor B, the oxyanion-hole loop does not adopt the zymogen state. This indicates that proteolytic activity of factor B is probably not controlled directly, as in trypsinogens, but rather through quaternary rearrangement of the domains in the assembly process.

Triad of CCP domains
The three CCP domains of fragment Ba adopt an unexpected triad arrangement, with domains CCP2 and CCP3 packed tightly (**Supplementary Table 1** online) into an antiparallel dimer capped by CCP1. This arrangement produces a small hydrophobic core at the triad center (**Fig. 3b**). Changes in the CCP2-CCP3 interface reduce C3b binding and hemolytic activity[22,23], and antibodies directed against CCP1 and CCP3 block hemolytic activity[22,24] (**Supplementary Fig. 4** online), indicating that the triad of CCP domains provides an important binding site for C3b. Domain CCP1 probably hinders access of the ligand C3b to the Mg^{2+}-dependent MIDAS of the VWA domain (**Supplementary Fig. 5** online). Because the triad of CCP domains appears to be only weakly associated with the VWA and SP domains (**Supplementary Fig. 4** and **Supplementary Table 2** online), we hypothesize that binding of the CCP domains to C3b dislocates the CCP triad from the VWA and SP domains. Concomitantly, dislocation of the CCP triad may be coupled, through the short CCP3-αL connecting loop (**Fig. 3b**), to displacement of helix αL from its binding groove in the VWA domain.

DISCUSSION
Factor B is activated by binding surface–bound C3b and subsequent cleavage by factor D. Our data reveal the conformation that keeps

factor B locked in its proenzyme state. The structure adds this locked conformation to the open and closed conformations described in past studies of the VWA and I domains[8,9] and provides insights into a previously uncharacterized mechanism for regulating serine protease activity[21]. Assembly of an active protease complex probably proceeds through a number of steps. We hypothesize that initial binding of C3b dislocates the CCP triad. In turn, dislocation of the CCPs probably induces formation of an active MIDAS and allows access of the large C3b ligand. Concomitantly, the blocking helix αL is displaced from its position in the VWA domain, thereby allowing the activation helix α7 to move into its normal location. Rearrangement of helices αL and α7 liberates the bound scissile peptide, making it accessible for proteolytic cleavage by factor D. Cleavage of the scissile bond results in dissociation of the Ba fragment, yielding the active, short-lived protease complex that cleaves C3 into C3a and C3b. Thus, the tight regulation of complement activation is determined by a series of conformational changes that establish the C3 convertase activity required for amplification, which is crucial for the biological functions of the complement system.

METHODS

Protein expression, purification and crystallization. Human factor B fused to an N-terminal Gly-Ser-(His)$_6$-Gly-Ser tag was expressed in human embryonic kidney 293S GnTI$^-$ cells to prevent complex and heterogeneous N-linked glycosylation[25]. Secreted factor B was purified from the expression medium via immobilized metal affinity chromatography followed by size-exclusion chromatography. The purified protein showed a single band of 90 kDa on Coomassie-stained SDS-PAGE gels and on western blots probed with an antibody to His$_6$. Details of factor B expression and purification are given in **Supplementary Methods** online. Crystals were grown by hanging drop vapor diffusion by mixing 1 µl factor B (13 mg ml^{-1}) in 10 mM tris(hydroxymethyl)

aminomethane (pH 7.4), 25 mM arginine, 25 mM glutamic acid and 1 µl well solution (50 mM malic acid 2-(N-morpholino)ethanesulfonic acid tris (hydroxymethyl)aminomethane buffer (pH 6.5) and 12% (w/v) PEG 1,500) at 20 °C. Glycerol (20% v/v) was added to the well solution before flash-cooling of the crystal in liquid nitrogen. The crystal diffracted to 2.3-Å resolution at the European Synchrotron Radiation Facility beamline ID14-EH4. The space group of the crystal was identified as $P3_1 21$ ($a = b = 104.0$ and $c = 151.1$ Å). Data were processed by MOSFLM and CCP4 (ref. 26). Crystallographic data collection and refinement statistics are given in **Table 1**.

Structure determination. The SP and VWA domain were placed by molecular replacement using Phaser[27] with structures of the isolated SP (PDB 1DLE)[28] and VWA (PDB 1Q0P)[14] domains of factor B as search models. Subsequent placement of the three CCP domains using various homologous structures, as well as model completion by automated model building using ARP/wARP[29], failed at this stage. The VWA helix α7 and SP domain loops C and D were rebuilt and the partial model was refined using COOT[30], RESOLVE[31] and REFMAC5 (ref. 32). Using this partial model, ARP/wARP then successfully completed the model to ~80%. Iterative cycles of refinement with REFMAC5 and model building in COOT were used to finalize the model. The refined model of factor B contains 710 residues; residues 1–8, 218–232, 321–326 and 344–346 were excluded from the model because of poor electron density. R and R_{free} values were 19.5% and 24.1%, respectively (see **Table 1** for refinement statistics). All molecular graphic figures were generated with PyMOL (http://pymol.sourceforge.net).

Accession codes. Protein Data Bank: Coordinates and structure factors have been deposited with accession code 2OK5.

Note: Supplementary information is available on the Nature Structural & Molecular Biology website.

Table 1 Data collection and refinement statistics

	Factor B
Data collection	
Space group	$P3_1 21$
Cell dimensions	
a, b, c (Å)	104.0, 104.0, 151.1
α, β, γ (°)	90, 90, 120
Resolution (Å)	60.0–2.3 (2.42–2.30)
R_{merge}	10.8 (56.1)
$I / \sigma I$	10.4 (2.6)
Completeness (%)	99.8 (100)
Redundancy	4.1 (4.1)
Refinement	
Resolution (Å)	60.0–2.30
No. reflections	40,409
R_{work} / R_{free}	0.195 / 0.241
No. atoms	
Protein	5,745
Ligand/ion	78
Water	295
B-factors (Å^2)	
Protein	33.5
Ligand/ion	58.1
Water	31.6
R.m.s. deviations	
Bond lengths (Å)	0.010
Bond angles (°)	1.30

Values in parentheses are for highest-resolution shell.

1. Carroll, M.C. The complement system in regulation of adaptive immunity. *Nat. Immunol.* **5**, 981–986 (2004).
2. Walport, M.J. Complement. First of two parts. *N. Engl. J. Med.* **344**, 1058–1066 (2001).
3. Fishelson, Z., Pangburn, M.K. & Muller-Eberhard, H.J. Characterization of the initial C3 convertase of the alternative pathway of human complement. *J. Immunol.* **132**, 1430–1434 (1984).
4. Xu, Y., Narayana, S.V. & Volanakis, J.E. Structural biology of the alternative pathway convertase. *Immunol. Rev.* **180**, 123–135 (2001).
5. Pangburn, M.K. & Muller-Eberhard, H.J. The C3 convertase of the alternative pathway of human complement. Enzymic properties of the bimolecular proteinase. *Biochem. J.* **235**, 723–730 (1986).
6. Pryzdial, E.L. & Isenman, D.E. Alternative complement pathway activation fragment Ba binds to C3b. Evidence that formation of the factor B-C3b complex involves two discrete points of contact. *J. Biol. Chem.* **262**, 1519–1525 (1987).
7. Horiuchi, T., Macon, K.J., Engler, J.A. & Volanakis, J.E. Site-directed mutagenesis of the region around Cys-241 of complement component C2. Evidence for a C4b binding site. *J. Immunol.* **147**, 584–589 (1991).
8. Emsley, J., Knight, C.G., Farndale, R.W., Barnes, M.J. & Liddington, R.C. Structural basis of collagen recognition by integrin alpha2beta1. *Cell* **101**, 47–56 (2000).
9. Springer, T.A. Complement and the multifaceted functions of VWA and integrin I domains. *Structure* **14**, 1611–1616 (2006).
10. Ponnuraj, K. *et al.* Structural analysis of engineered Bb fragment of complement factor B: insights into the activation mechanism of the alternative pathway C3-convertase. *Mol. Cell* **14**, 17–28 (2004).
11. Milder, F.J. *et al.* Structure of complement component C2a: implications for convertase formation and substrate binding. *Structure* **14**, 1587–1597 (2006).

12. Smith, C.A., Vogel, C.W. & Muller-Eberhard, H.J. MHC Class III products: an electron microscopic study of the C3 convertases of human complement. *J. Exp. Med.* **159**, 324–329 (1984).

13. Shimaoka, M. *et al.* Structures of the alpha L I domain and its complex with ICAM-1 reveal a shape-shifting pathway for integrin regulation. *Cell* **112**, 99–111 (2003).

14. Bhattacharya, A.A., Lupher, M.L., Jr., Staunton, D.E. & Liddington, R.C. Crystal structure of the A domain from complement factor B reveals an integrin-like open conformation. *Structure* **12**, 371–378 (2004).

15. Emsley, J., King, S.L., Bergelson, J.M. & Liddington, R.C. Crystal structure of the I domain from integrin alpha2beta1. *J. Biol. Chem.* **272**, 28512–28517 (1997).

16. Fishelson, Z., Pangburn, M.K. & Muller-Eberhard, H.J. C3 convertase of the alternative complement pathway. Demonstration of an active, stable C3b, Bb (Ni) complex. *J. Biol. Chem.* **258**, 7411–7415 (1983).

17. Hourcade, D.E., Mitchell, L., Kuttner-Kondo, L.A., Atkinson, J.P. & Medof, M.E. Decay-accelerating factor (DAF), complement receptor 1 (CR1), and factor H dissociate the complement AP C3 convertase (C3bBb) via sites on the type A domain of Bb. *J. Biol. Chem.* **277**, 1107–1112 (2002).

18. Hourcade, D.E., Mitchell, L.M. & Oglesby, T.J. Mutations of the type A domain of complement factor B that promote high-affinity C3b-binding. *J. Immunol.* **162**, 2906–2911 (1999).

19. Williams, S.C., Hinshelwood, J., Perkins, S.J. & Sim, R.B. Production and functional activity of a recombinant von Willebrand factor-A domain from human complement factor B. *Biochem. J.* **342**, 625–632 (1999).

20. Kam, C.M. *et al.* Human complement proteins D, C2, and B. Active site mapping with peptide thioester substrates. *J. Biol. Chem.* **262**, 3444–3451 (1987).

21. Khan, A.R. & James, M.N. Molecular mechanisms for the conversion of zymogens to active proteolytic enzymes. *Protein Sci.* **7**, 815–836 (1998).

22. Hourcade, D.E., Wagner, L.M. & Oglesby, T.J. Analysis of the short consensus repeats of human complement factor B by site-directed mutagenesis. *J. Biol. Chem.* **270**, 19716–19722 (1995).

23. Xu, Y. & Volanakis, J.E. Contribution of the complement control protein modules of C2 in C4b binding assessed by analysis of C2/factor B chimeras. *J. Immunol.* **158**, 5958–5965 (1997).

24. Thurman, J.M. *et al.* A novel inhibitor of the alternative complement pathway prevents antiphospholipid antibody-induced pregnancy loss in mice. *Mol. Immunol.* **42**, 87–97 (2005).

25. Reeves, P.J., Callewaert, N., Contreras, R. & Khorana, H.G. Structure and function in rhodopsin: high-level expression of rhodopsin with restricted and homogeneous N-glycosylation by a tetracycline-inducible N-acetylglucosaminyltransferase I-negative HEK293S stable mammalian cell line. *Proc. Natl. Acad. Sci. USA* **99**, 13419–13424 (2002).

26. Collaborative Computational Project, Number 4. The CCP4 suite: programs for protein crystallography. *Acta Crystallogr. D Biol. Crystallogr.* **50**, 760–763 (1994).

27. Storoni, L.C., McCoy, A.J. & Read, R.J. Likelihood-enhanced fast rotation functions. *Acta Crystallogr. D Biol. Crystallogr.* **60**, 432–438 (2004).

28. Jing, H. *et al.* New structural motifs on the chymotrypsin fold and their potential roles in complement factor B. *EMBO J.* **19**, 164–173 (2000).

29. Perrakis, A., Morris, R. & Lamzin, V.S. Automated protein model building combined with iterative structure refinement. *Nat. Struct. Biol.* **6**, 458–463 (1999).

30. Emsley, P. & Cowtan, K. Coot: model-building tools for molecular graphics. *Acta Crystallogr. D Biol. Crystallogr.* **60**, 2126–2132 (2004).

31. Terwilliger, T.C. Automated main-chain model building by template matching and iterative fragment extension. *Acta Crystallogr. D Biol. Crystallogr.* **59**, 38–44 (2003).

32. Winn, M.D., Isupov, M.N. & Murshudov, G.N. Use of TLS parameters to model anisotropic displacements in macromolecular refinement. *Acta Crystallogr. D Biol. Crystallogr.* **57**, 122–133 (2001).

33. Janssen, B.J., Christodoulidou, A., McCarthy, A., Lambris, J.D. & Gros, P. Structure of C3b reveals conformational changes that underlie complement activity. *Nature* **444**, 213–216 (2006).

34. Wiesmann, C. *et al.* Structure of C3b in complex with CRIg gives insights into regulation of complement activation. *Nature* **444**, 217–220 (2006).